

Experimental Searches for the Axion and Axion-like Particles

Peter W. Graham,¹ Igor G. Irastorza,² Steven K. Lamoreaux,³ Axel Lindner,⁴ and Karl A. van Bibber,⁵

¹Corresponding author, Stanford Institute for Theoretical Physics, Stanford University, Stanford, CA, USA, 94305

²Laboratorio de Física Nuclear y Astropartículas, Departamento de Física Teórica, Universidad de Zaragoza, 50009 Zaragoza, Spain

³Department of Physics, Yale University, New Haven, CT, USA, 06511

⁴DESY, Notkestraße 85, 22607 Hamburg, Germany

⁵Department of Nuclear Engineering, University of California Berkeley, Berkeley CA, USA 94720

Xxxx. Xxx. Xxx. Xxx. YYYY. AA:1–31

This article's doi:
10.1146/((please add article doi))

Copyright © YYYY by Annual Reviews.
All rights reserved

Keywords

axion, axion-like particles, dark matter, microwave cavity, NMR, helioscope, photon regeneration

Abstract

Four decades after its prediction, the axion remains the most compelling solution to the Strong-CP problem and a well-motivated dark matter candidate, inspiring a host of elegant and ultrasensitive experiments based on axion-photon mixing. This report reviews the experimental situation on several fronts. The microwave cavity experiment is making excellent progress in the search for dark matter axions in the microelectronvolt range and may be plausibly extended up to 100 μeV . Within the past several years however, it has been realized that axions are pervasive throughout string theories, but with masses that fall naturally in the nanoelectronvolt range, for which a NMR-based search is under development. Searches for axions emitted from the Sun's burning core, and purely laboratory experiments based on photon regeneration have both made great strides in recent years, with ambitious projects proposed for the coming decade. Each of these campaigns has pushed the state of the art in technology, enabling large gains in sensitivity and mass reach. Furthermore each modality has also been exploited to search for more generalized axion-like particles, that will also be discussed in this report. We are hopeful, even optimistic, that the next review of the subject will concern the discovery of the axion, its properties, and its exploitation as a probe of early universe cosmology and structure formation.

Contents

1. Introduction	2
2. Strong-CP and the Axion	3
2.1. Axion-like particles and other WISPs	6
3. Searches for Dark Matter Axions	6
3.1. Axionic dark matter	6
3.2. Cavity microwave experiment	7
3.3. ADMX and ADMX-HF	9
3.4. Detection with NMR: CASPER	13
4. Searches for Solar Axions	16
4.1. Solar Axions	16
4.2. Axion helioscopes	18
4.3. CAST	19
4.4. IAXO	21
5. Purely Laboratory Experiments	22
5.1. LSW experiments with microwaves, optical photons and X-rays	23
5.2. The future of LSW experiments	24
6. Summary and Conclusions	26

1. Introduction

Since its prediction in 1978 (1, 2), there has been a steady crescendo of interest in the axion, and a coordinated global effort to find it is now finally taking shape. Should it ultimately be discovered, it would finally resolve one of the last outstanding questions in the Standard Model of particle physics, namely it would validate the Peccei-Quinn mechanism to protect the strong interaction from CP-violating effects (3, 4), as evidenced by the absence of a neutron electric dipole moment. Furthermore, it may be discovered as the dark matter halo of our Milky Way galaxy, thus answering the question of what constitutes the predominant form of matter in our Universe. This will be an experimental review, focusing on new concepts and developments since the last such report in this journal (5) and in others (6, 7). The reader is referred to several excellent theory reviews (8, 9, 10, 11, 12) that are still largely up to date. There is one new development of interest to our present purpose however, namely the realization that any string theory contains several and perhaps a large number of axion-like particles, although they are extremely light, of order neV . This will be discussed briefly in Sec. 3.4, before describing the NMR-based experiment to search that mass region. Nevertheless, some theoretical preliminaries are in order, therefore this review will begin with the basic physics underlying the axion and its phenomenology in Sec. 2. Constraints on the axion's mass and couplings primarily from its cosmological production and astrophysics will be introduced at the beginning of Sec. 3 to prepare for the discussion of the microwave cavity experiment. Axion-photon mixing within a magnetic field in the relativistic limit relevant both to the solar searches and laboratory experiments will be presented at the beginning of Sec. 4, along with axion emission from the Sun's burning core.

While this review primarily concerns the axion solving the strong-CP problem, more generalized axion-like particles (ALPs) accessible to these experiments will also be dealt with. As we are writing from the experimental perspective, after all, one should be open to

surprises!

2. Strong-CP and the Axion

The gauge sector of the Standard Model of electroweak interactions is among the most successful theories in the history of physics, while the flavor sector is still incomplete with known issues and uncertainties, *e.g.*, the neutrino mass spectrum. Perhaps the most mysterious issue is that of the so-called strong CP problem (combined charge conjugation C and parity inversion P symmetry, or equivalently time reversal T symmetry) – why does the quantum chromodynamic (QCD) Lagrangian conserve CP symmetry (or equivalently time reversal T symmetry) apparently perfectly, to within extraordinarily strict experimental limits, when there is no fundamental reason to exclude possible symmetry nonconserving interactions?

As described in (13), this problem can be understood as follows: The Lagrangian of the electromagnetic field

$$-\frac{1}{4}F_{\mu\nu}F_{\mu\nu} = \frac{1}{2}(\vec{E}^2 - \vec{B}^2) \quad (1)$$

can comprise other Lorentz scalars, such as (14)

$$F_{\mu\nu}\tilde{F}_{\mu\nu}, \quad \tilde{F}_{\mu\nu} = \frac{1}{2}\epsilon_{\mu\nu\kappa\lambda}F_{\kappa\lambda}. \quad (2)$$

This scalar violates both P and T invariance, as evident from its three dimensional form:

$$F_{\mu\nu}\tilde{F}_{\mu\nu} = -4\vec{E} \cdot \vec{B}. \quad (3)$$

However this scalar generates no observable effects in electrodynamics because it is a 4-divergence and the fields fall off rapidly toward infinity.

The corresponding possible P and T violating term in the QCD Lagrangian is usually written as

$$L_\theta = -\theta(\alpha_s/8\pi)\tilde{G}_{\mu\nu}^a G_{\mu\nu}^a \quad (4)$$

and is called the θ term, where $\alpha_s \sim 1$ is the coupling constant for the gluon field G , and is the QCD analogue of the fine structure constant $\alpha = 1/137$ in electrodynamics. While the four-divergence of this term can remain zero, implying that dynamics are not directly affected by it, both the chiral anomaly and the self-interaction of the gluon vector potential field configurations, which do not fall off rapidly enough at infinity, can lead to observable effects.

Most famously, the θ term provides a contribution to the neutron electric dipole moment (EDM) which is estimated in (15, 16). First, a chiral rotation $\psi \rightarrow \exp(-i\gamma_5\theta)\psi$ of the quark spinor fields ψ transforms the θ term away. Under this rotation, the mass term in the Hamiltonian of the light quarks, u , d , s ,

$$m_u\bar{u}u + m_d\bar{d}d + m_s\bar{s}s \quad (5)$$

acquires a CP -odd term

$$\delta H_{CP} = i\theta \frac{m_u m_d m_s}{m_u m_d + m_u m_s + m_d m_s} (\bar{u}\gamma_5 u + \bar{d}\gamma_5 d + \bar{s}\gamma_5 s). \quad (6)$$

Because the s quark is much heavier than u and d , the mass factor simplifies to

$$\frac{m_u m_d m_s}{m_u m_d + m_u m_s + m_d m_s} \approx \frac{m_u m_d}{m_u + m_d}. \quad (7)$$

The CP -odd πNN vertex generated by this Hamiltonian can be transformed by use of the PCAC technique to

$$\langle \pi^a N_f | \delta H_{CP} | N_i \rangle = -\theta \frac{m_u m_d}{m_u + m_d} \frac{\sqrt{2}}{f_\pi} \langle N_f | \bar{q} \tau^a q | N_i \rangle \quad (8)$$

where τ^a is the isotopic spin operator and $f_\pi = 130$ MeV is the pion decay constant. The nucleon matrix element $\langle p | \bar{u}d | n \rangle$ is related through SU(3) symmetry to the mass splitting in the baryon octet:

$$\langle p | \bar{u}d | n \rangle = \bar{p}n \frac{M_\Xi - M_\Sigma}{m_s} \approx \bar{p}n \quad (9)$$

where p and n are the Dirac spinors of the proton and neutron; M_Ξ and M_Σ are the masses of the Ξ and Σ hyperons, respectively. The full πNN interaction can now be described by an effective Hamiltonian

$$H_{\pi NN} = \vec{\pi} \vec{N} \vec{\tau} (i \gamma_5 g_{\pi NN} + \bar{g}_{\pi NN}) N, \quad (10)$$

where the CP -odd constant is

$$\bar{g}_{\pi NN} = -\theta \frac{m_u m_d}{m_u + m_d} \frac{\sqrt{2}}{f_\pi} \frac{M_\Xi - M_\Sigma}{m_s} \approx -0.027\theta. \quad (11)$$

The CP -even πNN constant in the effective Hamiltonian is known,

$$g_{\pi NN} = 13.6. \quad (12)$$

In (16), a crucial observation is made. In the chiral limit $m_\pi \rightarrow 0$ the neutron EDM can be expressed exactly via $\bar{g}_{\pi NN}$ and $g_{\pi NN}$. In this limit, there are only two diagrams that are singular in the pion mass and thus contribute to the EDM. In these diagrams, a πNN vertex is the strong pseudoscalar coupling, with the coupling constant $g_{\pi NN} \sqrt{2}$, and the second is a CP -odd scalar, with the coupling constant $\bar{g}_{\pi NN} \sqrt{2}$. The contribution of these diagrams to the neutron EDM is

$$d_n = \frac{|e|}{m_p} \frac{g_{\pi NN} \bar{g}_{\pi NN}}{4\pi^2} \ln \frac{m_\rho}{m_\pi} = -3.3 \times 10^{-16} \theta [e \cdot \text{cm}]. \quad (13)$$

The choice of the ρ meson mass $m_\rho = 770$ MeV as the typical hadronic scale at which the logarithmic integral is cut off is somewhat arbitrary. The chiral parameter, the logarithm in Eq. (13), is not large for any reasonable cut-off and is only 1.7 when m_ρ is used. Due to the absence of other terms logarithmic in m_π , a coincidental mutual cancellation between this contribution and possible others appears as unlikely. Therefore Eq. (13) can be considered a conservative estimate of the neutron EDM.

Combining this estimate with the most sensitive experimental result given in Ref. (17), $d_n < 2.9 \times 10^{-26}$ e-cm, sets a very strict upper limit for the CP -odd QCD parameter

$$|\theta| < 9 \times 10^{-11}. \quad (14)$$

This is the strong CP problem: There is no natural explanation for the extreme smallness of the parameter θ and is considered to be a fine-tuning problem. Indeed, it appears as particularly unnatural when one considers that θ is renormalized by other CP -odd interactions (e.g., known CP violation in K meson decay), and in general its renormalization

can be infinite. It has been shown that, in the Standard Model, the induced contributions to θ almost certainly diverge logarithmically starting at 14th(!) order in the electroweak coupling constant (18, 19). Therefore, as a technicality, θ cannot be calculated.

One solution to this problem, which is quite obvious from Eq. (6), is to assume that one of the quark masses is zero or very small (lighter than a neutrino). This assumption apparently contradicts experimental data, although that is not entirely certain.

A solution to the strong CP problem that has wide interest, particularly in the context of this Review, is to leave the θ term as it is, but to somehow make it irrelevant. This is achieved by introducing an extra global symmetry into the theory (3, 4), *i.e.*, by considering θ as a field, not a fixed parameter. Such a symmetry leads in turn to the prediction of a new light pseudoscalar particle, the axion (1, 2). In a restricted sense, the axion plays a role similar to the Higgs boson; the CP violating interaction cannot be calculated in the context of the Standard Model and in fact diverges without the axion, while electroweak interactions beyond first order diverge without the (now discovered!) Higgs boson. Of course it would be incorrect to say that the axion is as well motivated as the Higgs boson, however the parallelism should be noted.

The mass of the axion is unknown, but is bound from both above and from below by experiments and observations.

Essentially all of the physics of the axion depends on a large unknown energy scale f_a , at which Peccei-Quinn symmetry is broken; in the low-energy limit of their theory, the non-perturbative vacuum structure of QCD drives the parameter of the CP-violating term, to the CP-conserving minimum, with the axion resulting from the remnant oscillations of the axion field about this minimum. The mass of the axion is given by (9, 10, 11):

$$m_a \approx 6 \text{ eV} \left(\frac{10^6 \text{ GeV}}{f_a} \right) \quad (15)$$

In its original form, the PQ symmetry-breaking scale was posited (for no compelling reason) to be of order the electroweak scale, f_{EW} , implying very heavy axions (~ 100 keV) which were quickly ruled out by accelerator- and reactor-based experiments. More general models were then constructed of much higher values of f_a and much smaller m_a .

Generically, all the couplings of the axion to radiation and matter are also inversely proportional to f_a . The axion-photon coupling is of special interest here, as virtually all of the most sensitive search strategies are based on the coherent mixing of axions and photons in a strong magnetic field. Being a pseudoscalar ($J^\pi = 0^-$), the axion has a two-photon coupling whose strength is given by:

$$g_{a\gamma\gamma} = \frac{\alpha g_\gamma}{\pi f_a} \quad (16)$$

where g_γ is a dimensionless model-dependent parameter of order unity; $g_\gamma = -0.97$ in the KSVZ model (20, 21), and $g_\gamma = 0.36$ in the DFSZ model (22, 23). These values are representative within broad classes of hadronic and GUT-inspired axions, underlining an important feature of the theory that the dimensionless axion-photon coupling g_γ is highly insensitive to the specific axion model. This observation extends even to axions ubiquitous within string theory, and which are perhaps even intrinsic to their structure (24)¹.

¹This paper erroneously implies $g_\gamma^{\text{STRING}} = (1/4)g_\gamma^{\text{DFSZ}}$; however the author subsequently clarified that g_γ within string models should be *exactly* equal to that of the most generic model, DFSZ, and represents a strict lower limit to the coupling. E. Witten, private communication (2007)

2.1. Axion-like particles and other WISPs

As explained above there is a strong physics case for the axion, but it may be just a first representative of a new particle family of so called Weakly Interacting Slim Particles (WISPs). Such WISPs are motivated for example by string-theory inspired extensions of the Standard Model, which predict, among others, the existence of axion-like particles (ALPs) and hidden photons (HPs) (25). While entirely unrelated to the Strong-CP problem, ALPs and HPs may also be viable dark matter candidates (26, 27). ALPs are of special interest, because there are a number of different astrophysics phenomena like the transparency of the universe to TeV photons (28, 29) and evolution of stars (30, 31), which might point to the existence of very light ALPs with a coupling strength detectable at the next generation of helioscopes and purely laboratory experiments. It should be stressed that the ongoing discussion on the validity of Naturalness (questioning arguments for the existence of new particles based on fine tuning issues) triggered by the results of the first run of LHC (see (32, 33) for example) does not influence the hints for WISPs as sketched here. Thus the parameter space for very light and very feebly interacting particles is opening up next to the axion region and experiments are encouraged to widen their field of view accordingly.

3. Searches for Dark Matter Axions

3.1. Axionic dark matter

A sufficiently light axion represents an excellent dark-matter candidate (34), as its density relative to the critical density of the universe is given by

$$\Omega_a \approx \left(\frac{6 \mu\text{eV}}{m_a} \right)^{\frac{7}{6}} \quad (17)$$

An axion of $m_a \approx 20 \mu\text{eV}$ (within a factor of ~ 2) would thus account for the entire dark matter density of the universe, $\Omega_m \approx 0.23$. Without tuning of the initial misalignment angle much lighter axions would overclose the universe, and therefore $m_a \approx 1 \mu\text{eV}$ may be taken as a strong lower limit on the axion mass, m_a . There has been a lingering controversy about the relative contribution between axion production from the vacuum realignment mechanism and radiation from topological defects (axion strings, domain walls). A definitive resolution is unlikely soon, but the current general consensus is that the sum of all contributions to Ω_a could push the axion mass corresponding to Ω_{DM} two orders of magnitude higher. As we are presently interested only in establishing conservative ranges for experiments searches should plan on reaching the μeV scale. Cosmology also provides an upper bound on the axion mass by the production of thermal axions, the hot dark matter limit of about 1 eV, but this does not concern us here.

Stellar evolution also places strict limits on axions (35). Axions of mass exceeding ~ 16 meV would have quenched the neutrino pulse observed from SN1987a, thus bounding the axion mass from above. The best indirect stellar bound on the axion-photon coupling comes from Galactic Globular Clusters, $g_{a\gamma\gamma} < 0.66 \times 10^{-10} \text{ GeV}^{-1}$, recently surpassing the best direct stellar bound, the CAST search for solar axions, $g_{a\gamma\gamma} \approx 0.88 \times 10^{-10} \text{ GeV}^{-1}$ discussed in Sec. 4. For Peccei-Quinn axions, such couplings correspond to masses far in excess of the open mass region, i.e. $10^{-6} \text{ eV} < m_a < 10^{-2} \text{ eV}$, and thus are not germane to the dark matter problem. There has been a modest literature in recent years suggesting that the luminosity function of white dwarfs (degenerate stars undergoing gravothermal cooling)

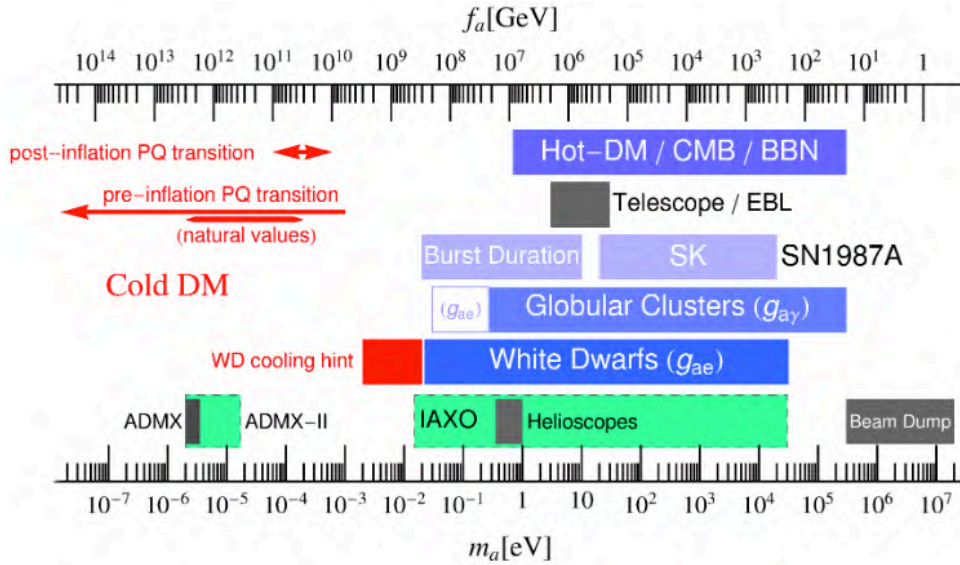


Figure 1

Limits on the axion mass established by cosmology and astrophysics. Light grey regions are very model dependent. (From Ref. (39).)

may require an additional cooling mechanism that could be accounted for by axions in the ~ 10 meV range (36, 37, 38). The evidence is far from compelling, not to mention that such masses are beginning to encroach in the region disfavored by SN1987a.

The range $10^{-(6-2)}$ eV is traditionally been regarded as the open mass window for axions; see Figure 1 (39). However, as previously mentioned, string theories are replete with axions or axion-like particles, upwards of a hundred within any particular realization, but such theories naturally favor $f_a \approx 10^{(15-16)}$ GeV, corresponding to neV-scale masses. It is impossible to say which, if any of these solve the Strong-CP problem, and which, if any would be cosmologically significant. String theory axions and possible limits from isocurvature fluctuations will be reviewed briefly in Sec. 3.4 as a preamble to the discussion of the NMR-based experiment, CASPER.

3.2. Cavity microwave experiment

Problematically such light axions would be so weakly coupled as to be undetectable in conventional experiments. In 1983, Pierre Sikivie resolved this conundrum by showing that axions constituting the Milky Way halo could resonantly convert into a monochromatic microwave signal in a high-Q microwave cavity permeated by a strong magnetic field (40, 41), with the conversion power given by

$$P_{\text{SIG}} = \eta g_{a\gamma\gamma}^2 \left(\frac{\rho_a}{m_a} \right) B_0^2 V C Q_L \quad (18)$$

The physics parameters, beyond the control of the experimentalist, are the axion-photon coupling constant $g_{a\gamma\gamma}$, the axion mass m_a , and the local density of axions in the halo, ρ_a .

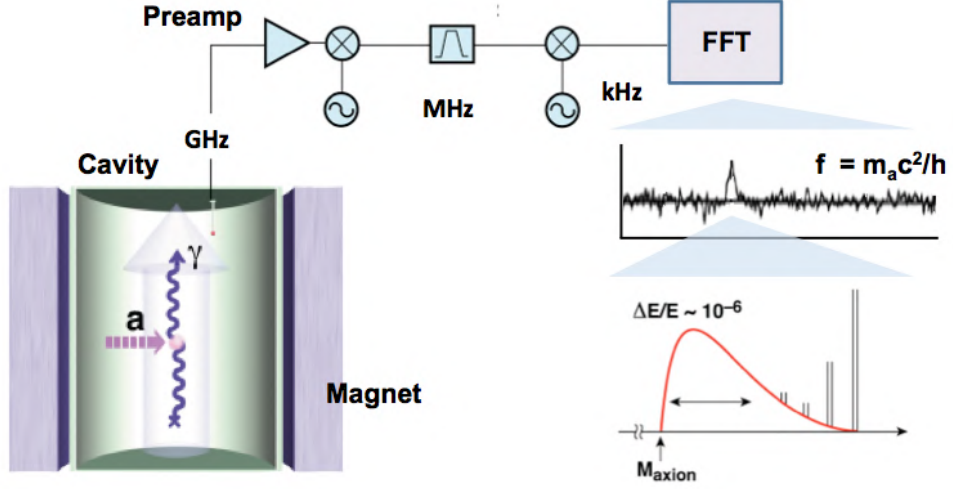


Figure 2

Schematic of the microwave cavity search for dark matter axions. Axions resonantly convert to a quasi-monochromatic microwave signal in a high-Q cavity in a strong magnetic field; the signal is extracted from the cavity by an antenna, amplified, mixed down to the audio range, and the power spectrum calculated by a FFT. Possible fine structure on top of the thermalized axion spectrum would reveal important information about the formation of our galaxy.

Within experimental control are the magnetic field strength B_0 , and the volume of the cavity V , as well as the mode-dependent form-factor C , and loaded quality factor of the cavity Q_L , i.e. the quality factor with power coupled out to the receiver. η is the fraction of power coupled out by the antenna probe, generally adjusted to be at or near critical coupling, $\eta = 1/2$. The resonant conversion condition is that the frequency of the cavity must equal the mass of the axion, $h\nu = m_a c^2 [1 + \frac{1}{2}\mathcal{O}(\beta^2)]$, where $\beta \approx 10^{-3}$ is the galactic virial velocity. The signal is thus monochromatic to 10^{-6} . The search is performed by tuning the cavity in small overlapping steps (Figure 2).

The expected signal power is extraordinarily tiny, of order 10^{-22} W for the current experiment. Actual detection of the axion is the consummate signal-processing problem, governed by the Dicke radiometer equation (42)

$$\frac{S}{N} = \frac{P_{\text{SIG}}}{kT_{\text{SYS}}} \sqrt{\frac{t}{\Delta\nu}}, \quad (19)$$

where S/N is the signal to noise ratio, and the total system noise temperature $T_{\text{SYS}} = T + T_N$ is the sum of the physical temperature T and the intrinsic amplifier noise temperature T_N , with k the Boltzmann constant. The integration time is t , and the bandwidth of the axion signal is $\Delta\nu$, where it is assumed that the resolution of the spectral receiver is much better than the width of the axion signal.

One especially important feature about the microwave cavity search for axions that strongly differentiates it from WIMP searches, is that it is a total energy detector, i.e. the signal represents the instantaneous (mass + kinetic) energy of the axion. While the majority

of the signal strength will almost certainly be found in a broad quasi-Maxwellian distribution of width $\frac{\Delta\nu}{\nu} \sim 10^{-6}$, there has been a great deal of speculation and research over the past two decades about the phase space structure of the axion signal, caustics, fine structure due to late infall axions, etc. (43). A high resolution channel has been implemented on ADMX based on a Fast Fourier Transform (FFT) of an entire subspectrum, the basic unit of data collection, which can resolve structure down to the transform limit, e.g. $\frac{\Delta\nu}{\nu} \sim 10^{-11}$ for a 100-second run at 1 GHz. Due to the motion of the laboratory through the dark-matter halo ($v_{\text{ROT}} \sim 0.4$ km/sec, $v_{\text{ORB}} \sim 30$ km/sec), any fine structure would exhibit both diurnal and sidereal modulations in frequency. A little reflection makes it clear that should such fine structure be found, fitting the amplitude and phase of the diurnal and sidereal oscillation in frequency would uniquely determine each vector flow to high precision, truly opening the field of dark matter astronomy (44). While N-body simulations strongly support a hierarchical and chaotic picture of structure formation, these simulations themselves exhibit significant mesoscale substructure in phase space, which could be studied.

3.3. ADMX and ADMX-HF

3.3.1. Early experiments. Two pilot efforts in the 1-4 GHz range, at BNL (45, 46) and the University of Florida (47), were mounted soon after publication of the experimental concept. These employed cavities of a few liters volume, and the best conventional amplifiers at that time, e.g. Heterojunction Field Effect Transistor (HFET) amplifiers. With noise temperatures only in the $T_N \sim 3$ -20 K range, they did not have the sensitivity to reach Peccei-Quinn axions (Figure 3). Nevertheless, these two experiments developed much of the design philosophy and know-how about microwave cavities that the current experiments still build on today.

The CARRACK experiment in Kyoto marked another significant development in the history of the microwave cavity experiment. The goal of CARRACK was to achieve a dramatic reduction in the system noise temperature, both by reducing the physical temperature of the experiment down to ~ 15 mK with a ^3He - ^4He dilution refrigerator, and by utilizing a Rydberg-atom single-quantum detector in lieu of a standard linear amplifier to eliminate the amplifier noise contribution. Linear amplifiers are ultimately subject to an irreducible noise contribution, the Standard Quantum Limit, $kT_{\text{SQL}} = h\nu$. The Rydberg-atom single-quantum detector can effectively be thought of as a tunable “RF photomultiplier tube”, for which the photon interacts as a particle rather than a wave, thus circumventing the SQL. Tada et al. were able to measure the blackbody photon spectrum of the cavity at 2.527 GHz as a function of temperature all the way down to $T = 67$ mK, nearly a factor of two below the Standard Quantum Limit of $T_{\text{SQL}} \sim 120$ mK (48). From the technical perspective, CARRACK was successful, but ultimately proved too complex to be feasible as a production experiment.

3.3.2. Axion Dark Matter eXperiment (ADMX). Drawing on the experience from the Rochester-Brookhaven-Fermilab (RBF) and the University of Florida (UF) searches, the ADMX collaboration designed an experiment with the goal to reach KSVZ axions saturating our galactic halo, whose local density would be $\rho_a \sim 0.45$ GeV/cm³. This goal would be achieved both by a scale-up of the cavity volume by two orders of magnitude, and profiting from the steady improvement in the noise temperature of commercial HFET amplifiers.

The NbTi superconducting magnet has an inner bore 60 cm \times 110 cm, and sustains a

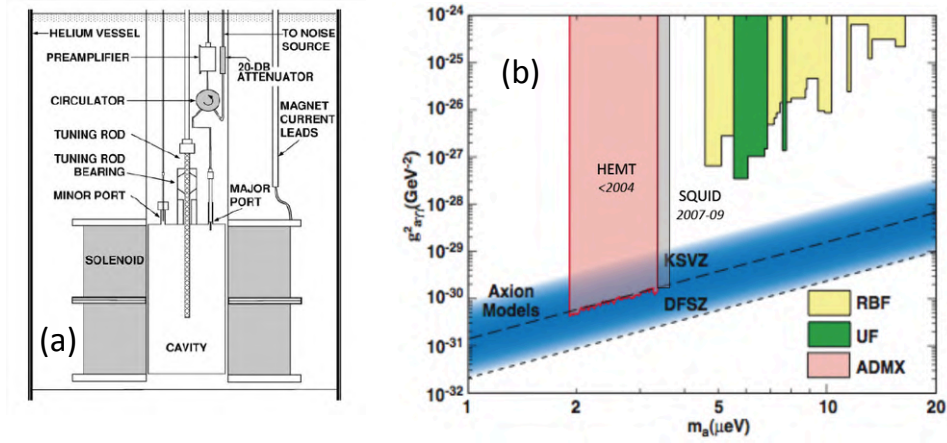


Figure 3

(a) Layout of the Rochester-Brookhaven-Fermilab (RBF) experiment (45, 46). (b) The 90% c.l. exclusion regions for the RBF, UF and ADMX experiments.

maximum central field of 8 T. The microwave cavities are made by electrodepositing high-purity copper on a stainless steel body, followed by annealing (Figure 4), leading to cavity quality factors of $Q \sim 10^5$; the experiment is tuned in small overlapping steps of the cavity bandpass. To date, the experiment has been cooled to superfluid helium temperatures, $T \sim 1.5$ K.

For the first operational phase of ADMX (1995-2004), HFET amplifiers made by NRAO were used, ultimately reaching a noise temperature $T_N \sim 1.5$ K, with the system noise temperature thus being $T_{SYS} \sim 3$ K. For the second operational phase (2007-09), Microstrip-coupled SQUID Amplifiers (MSA) developed specifically for ADMX were employed, whose noise temperature was demonstrated on the bench to be $T_N < 1.5 T_{SQL}$ at frequencies up to a GHz, when cooled to 30 mK (49, 50, 51). However, the noise of these MSAs exhibits a strong temperature dependence, and at pumped helium temperatures, are not better than transistor-based amplifiers; see Figure 4. Nevertheless, demonstrating that dc SQUID amplifiers could be made to work successfully in situ represented a great advance for the experiment, and a dilution refrigerator will be incorporated into the experiment in 2015, enabling the experiment to achieve $T_{SYS} < 200$ mK, sensitive to DFSZ axions even with less than saturation density.

To date, ADMX has covered 460 - 890 MHz in frequency (1.9 - 3.65 μeV) or slightly less than an octave in mass range (52, 53); Figure 3. This underscores the importance both of concurrent R&D on new cavity and amplifier concepts for frequencies much greater than a GHz, as well as greatly increasing the scanning rate of the experiment.

3.3.3. ADMX-HF (High Frequency). A second smaller ADMX platform has been constructed and commissioned at Yale, precisely to develop technologies and techniques applicable to the next higher decade in mass (54). The NbTi solenoidal magnet (9.4 T, 60 cm \times 110 cm) was designed for exceptionally high field uniformity ($B_r < 50$ G) for the purposes of testing thin-film superconducting cavities, although initially the cavity is elec-

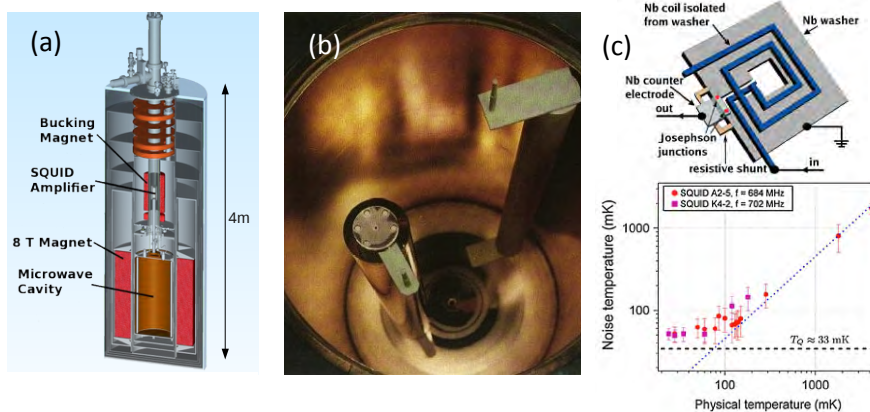


Figure 4

The Axion Dark Matter eXperiment. (a) Schematic layout. (b) Microwave cavity and tuning rods. (c) dc SQUID amplifiers. In addition to being near-quantum limited, the MSAs have been demonstrated to be tunable, work with a reactive load, and can be staged (49, 50, 51).

trodeposited copper (Figure 5). ADMX-HF incorporated a dilution refrigerator from the outset, resulting in a base temperature of the experiment $T \sim 25$ mK. Josephson Parametric Amplifiers (JPA) are well suited to the initial 5 GHz range of the experiment, where they possess high gain (20-30 dB), are tunable over an octave and can operate with a system noise temperature $T_N \sim T_{SQL}$ (55, 56); this noise was achieved within a factor of two in its first commissioning run. In its initial configuration, the experiment is projected to reach a sensitivity in axion-photon coupling $\sim 2 \times$ KSVZ.

Two promising lines of R&D are currently being pursued with high priority. The first is the prospect of incorporating Type-II superconducting thin films on all cylindrical surfaces of the microwave cavity to boost the Q by an order of magnitude, to which the axion-photon conversion power and thereby scanning rate are directly proportional. Xi et al. have recently demonstrated that very thin films of $\text{Nb}_x\text{Ti}_{1-x}\text{N}$ are perfectly microwave reflecting to frequencies > 100 GHz, immersed a magnetic field parallel to its surface up to $B_{\parallel} = 10$ T (57). Encouraged by this report, a program has been initiated of making and characterizing thin (10-200 nm) NbTiN films by RF plasma deposition. Satisfactory films on planar samples were readily achieved that are non-critical in exact composition (Figure 5). RF tests of small prototype cavities will be conducted next, and finally testing

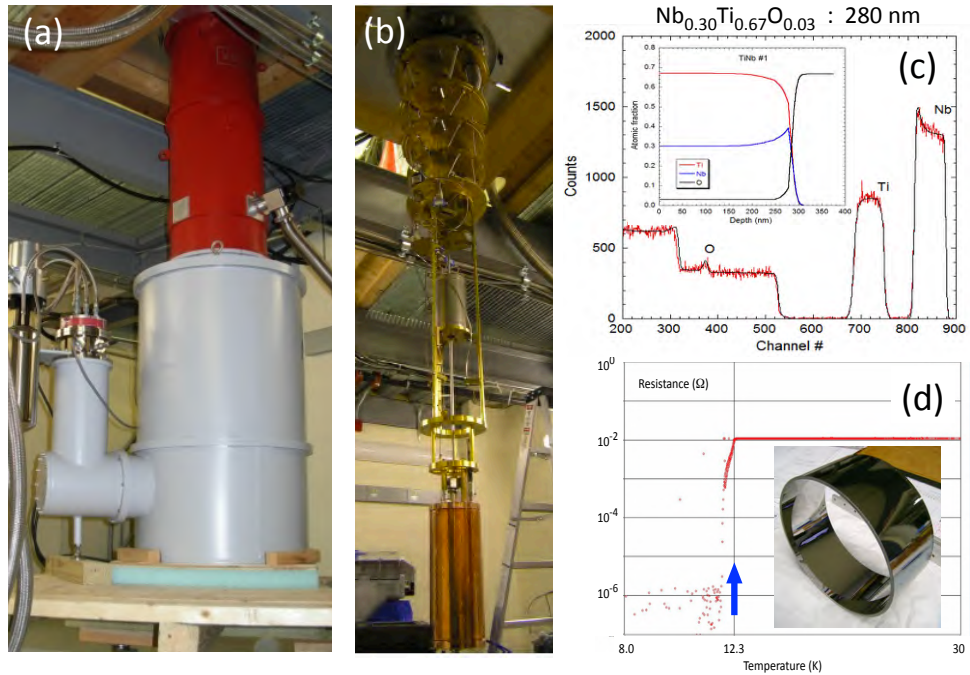


Figure 5

(a) ADMX-HF below deck, showing the magnet (grey) and dilution refrigerator (red). (b) Experimental gantry, showing the dilution refrigerator (top), the JPA magnetically shielded canister (middle) and microwave cavity (bottom). (c) Rutherford backscattering profile of a thin-film superconductor. (d) Resistance vs. temperature, demonstrating $T_C > 12$ K. (Insert) Thin-film superconductor deposited on the inside of a 10 cm diameter quartz tube.

them in a magnetic field. Successful implementation in ADMX-HF will require minimizing lossy flux vortices penetrating the superconducting surfaces; this requires the film be both extremely thin, and parallel to the magnetic field. To this end, the magnet was designed to meet strict specifications on field uniformity to minimize radial components.

The other major R&D effort will be the incorporation of a receiver based on squeezed-vacuum states to evade the quantum limit in noise, employed so far only by the laser interferometric gravity wave community, i.e. LIGO and GEO. The JILA group in ADMX-HF have used one JPA to measure the squeezed noise generated by a second JPA (58) achieving an equivalent noise temperature $T_N = h\nu/4$. Indeed, this experiment can be regarded as a proof-of-principle demonstration of a quantum-noise evading axion search. Not only was it possible to measure noise in one quadrature below the standard quantum limit, but also to demonstrate that quadrature had fluctuations below vacuum because it had been squeezed. The system noise could conceivably be reduced to 1/10 of the quantum limit. Together with the gain associated with the superconducting thin-film cavity, this small-volume experiment could ultimately reach DFSZ sensitivity.

Examining quantum noise in the cavity and amplifier more rigorously, Lamoreaux et al. have concluded that at higher frequencies, and thus higher axion masses, single-photon

detectors become competitive and ultimately favored, when compared to quantum-limited linear amplifiers, as the detector technology in the microwave cavity experiment (59), and that the cross-over point in this comparison is not far above the frequencies of the current ADMX-HF search range, of order 10 GHz. The microwave cavity experiment can profitably leverage advances in superconducting qubit readout schemes (60, 61, 62).

3.3.4. New Directions and Concepts. The past several years have seen a number of new search concepts for the detection of dark matter axions. The NMR-based experiment CASPER to explore the $10^{-(6-9)}$ eV mass range will be discussed separately in Sec. 3.4. However other promising innovations warrant brief mention here.

Rybka et al. have described an experiment designed on an open microwave resonator structure appropriate for axions in the 100 -1000 μeV decade, where the wavelength of the microwave photon after conversion ranges from $\lambda = 10 - 1$ mm (63). As the conversion probability maximizes strongly when the applied magnetic field $B(r)$ follows the electric field of the photon mode $E(r)$, a wiggler-like magnetic field is required with a continuously tunable periodicity to sweep out the range of masses. Rybka et al. effect this with a series of wire planes in the open resonator of alternating sign in current; ultimately these planes will consist of superconducting wires or stripes patterned on a thin substrate. A first prototype was able to exclude axions as the dark matter between 68.2 and 76.5 μeV , with couplings $g_{a\gamma\gamma} > 4 \times 10^{-7} \text{GeV}^{-1}$, not far removed from existing limits from laser-based limits, remarkably with a magnetic field of $|B| < 10$ gauss. Ultimately sensitivity to couplings of 10^{-15}GeV^{-1} should be achievable, below DFSZ axions for that mass range.

Sikivie et al. have focused on the other challenge of the microwave cavity experiment, namely extending the search downward in mass (64), where much below 10^{-6} eV (~ 250 MHz) the cavity and the magnet which encloses it become unfeasibly large. What they propose to circumvent this limitation is replacing the cavity with a lumped-parameter LC circuit external to the magnetic field, excited by a pickup loop inside the magnet threaded by the transverse B-field of the mode. Optimistically, the authors represent that with a magnet such as that of the the current ADMX, this technique would be maximally sensitive around 10^{-7} eV, probing the band of Peccei-Quinn axion models. If the concept can be fully developed and implemented, such a lumped-parameter LC circuit search for dark matter axions could bridge a key gap between where the cavity-based experiment and the NMR-based experiment may have difficulty in overlapping.

Other new and imaginative concepts have been put forward recently. These include instrumenting magnets of extreme aspect ratio, e.g. high energy dipoles, with microwave cavities (65) as well as a proposal for a dish-geometry resonator that would be both directional and broadband in frequency (66). Such a dish antenna in fact has already been implemented for a Hidden Photon dark matter search.

3.4. Detection with NMR: CASPER

The Cosmic Axion Spin Precession Experiment (CASPER) proposal aims to open a new direction in the experimental search for axion dark matter. CASPER will detect the spin precession caused by axion dark matter using nuclear magnetic resonance (NMR) techniques (67, 68). This novel approach complements existing efforts: ADMX is sensitive to the higher axion frequencies, whereas CASPER will cover the lower frequencies where the axion

arises from energies $f_a \sim 10^{15} \text{ GeV} - 10^{19} \text{ GeV}^2$. This range is very challenging for any other technique to reach, though some astrophysical techniques may be able to probe it (71, 72, 73). A detection in such an experiment would not only represent the discovery of dark matter but would also provide insights into the high-energy scales from which such an axion would arise, near fundamental scales such as the grand unification, Planck, or string scales.

Almost all axion experiments search for the coupling of the axion to photons. CASPER searches for two different couplings of the axion and thus naturally divides into two experiments: CASPER-Wind and CASPER-Electric. The Wind experiment searches for the ‘axion wind’ effect, the direct coupling of the axion to the spin of the nucleus (68). This is the pseudoscalar coupling

$$\mathcal{L} = \dots + g_{\text{aNN}} (\partial_\mu a) \bar{N} \gamma^\mu \gamma_5 N \quad (20)$$

which physically causes a precession of a nucleon spin around the spatial gradient of the local axion dark matter field (68). CASPER-Electric searches for the time-varying nucleon electric dipole moment (EDM) caused by the axion (67), which can be written as the coupling of the axion to nucleons

$$\mathcal{L} = \dots - \frac{i}{2} g_d a \bar{N} \sigma_{\mu\nu} \gamma_5 N F^{\mu\nu}. \quad (21)$$

where F is the field strength of electromagnetism. This coupling arises from the fundamental defining coupling of the QCD axion to gluons $\propto \frac{a}{f_a} G\tilde{G}$ (74). Both of these effects are time-varying because the background axion dark matter field a oscillates at a frequency equal to its mass. The CASPER idea could also be used to search for the coupling of the axion to electron spin but that does not appear sensitive enough to get beyond current limits in that parameter space (68). There has been a long history and significant recent interest in looking at such effects on nucleons and electrons (75, 76, 77).

The main idea behind CASPER is to use the time-varying nature of the effect (either EDM or wind) to cause precession of nuclear spins in a sample of material. The Larmor frequency of the nuclear spins is scanned by ramping the magnetic field and at the frequency corresponding to the mass of the axion an NMR signal is observed in the usual way using a precise magnetometer as in Figure 6. There are many choices of possible sample material which are beginning to be tested experimentally and explored theoretically (78, 79) to find the optimum.

The Wind experiment is technically simpler since it does not require an applied electric field and hence can be done using LXe as the sample for which the required NMR techniques have already been perfected. It can cover large parts of general axion (or axion-like particle) parameter space, many orders of magnitude beyond current constraints as in Figure 7. It also provides a stepping stone towards the CASPER-Electric experiment, as within the Wind experiment, many of the key technologies needed for the Electric experiment will be developed. CASPER-Electric requires a more complicated material such as a ferroelectric or polar crystal with a large internal electric field, but it has a better ultimate sensitivity, allowing it to reach all the way to the QCD axion over several orders of magnitude in frequency space that are unreachable by other techniques as in Figure 8³.

²It used to be argued that this range was disfavored by cosmology, but that requires specific assumptions about initial conditions which are easily violated, thus this range is allowed, see e.g. (69,

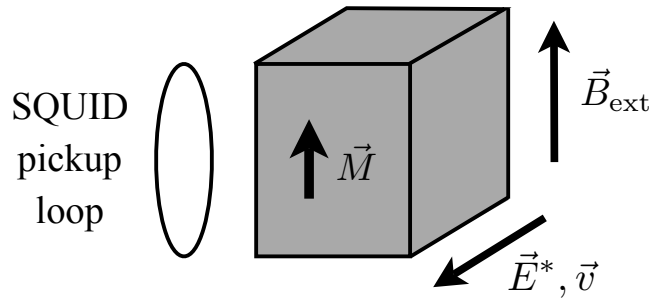


Figure 6

CASPER setup. The applied magnetic field \vec{B}_{ext} is colinear with the sample magnetization, \vec{M} . In CASPER-Wind the nuclear spins precess around the local velocity of the dark matter, \vec{v} , while in CASPER-Electric the nuclear EDM causes the spins to precess around an effective electric field in the crystal \vec{E}^* , perpendicular to \vec{B}_{ext} . The SQUID pickup loop is arranged to measure the transverse magnetization of the sample.

The CASPER-Wind experiment is in fact a search for any light particle that couples to nuclear spin (a generic coupling), not just the axion. For example, any pseudo-Goldstone boson is expected to possess a coupling that would be detectable in the CASPER-Wind experiment. It can also detect other types of dark matter, for example hidden photon dark matter (87, 26) is detectable through a nuclear dipole moment coupling.

Existing experiments may already be able to set limits on axion-like particles. Data from experiments searching for nuclear EDMs or looking at nucleon spin precession in a low background environment may be reanalyzed to search for a time-varying signal, a sign of the axion. While not ultimately as sensitive as CASPER where the signal is resonantly enhanced, such searches may be able to probe beyond the current astrophysical limits in Figures 7 and 8.

CASPER is a novel and highly sensitive search for a broad class of dark matter candidates in two new parameter spaces, the ‘axion wind’ and nuclear EDM, of which the QCD axion is the most well-known example. In particular, CASPER has the sensitivity to detect the QCD axion over a wide range of masses from $\sim 10^{-9}$ eV to 10^{-12} eV which are well-motivated by fundamental physics (24) and where no other experiment can detect it.

Construction is just beginning on the CASPER experiment. Work on CASPER is currently being carried out in several places including Stanford, Berkeley, and Mainz.

70), and is also well-motivated theoretically (24).

³Note that the Wind coupling leads to a spin-dependent force which could be probed using NMR techniques as well e.g. (80, 81, 82, 83, 84, 85, 86).

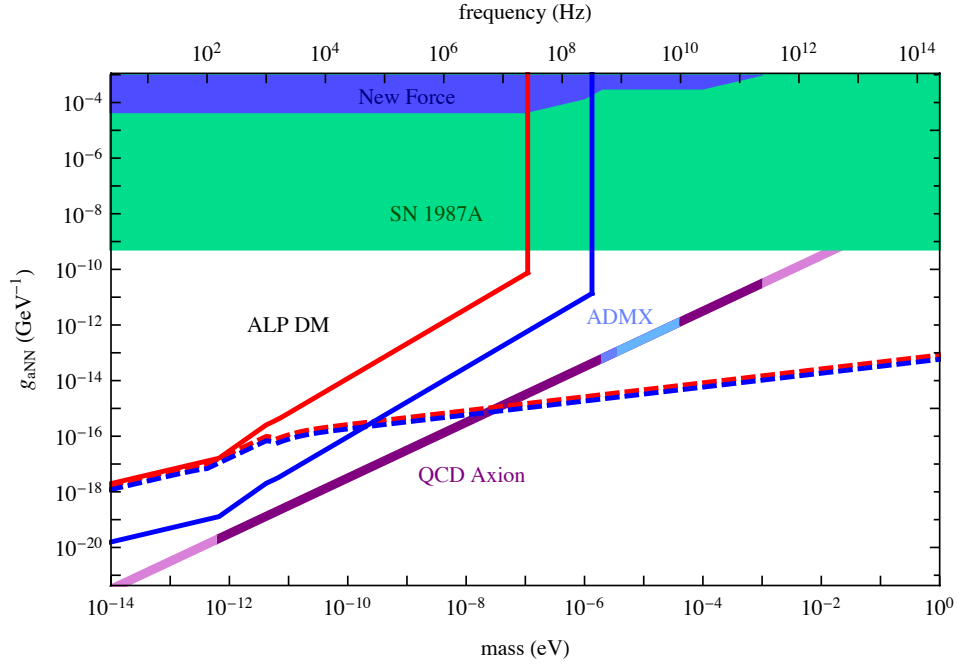


Figure 7

Sensitivity of the CASPER-Wind proposal. ALP parameter space in pseudoscalar coupling of axion to nucleons Eqn. 20 vs mass of ALP. The purple line is the region in which the QCD axion may lie. The width of the purple band gives an approximation to the axion model-dependence in this coupling. The darker purple portion of the line shows the region in which the QCD axion could be all of the dark matter and have $f_a < M_{\text{Pl}}$ as in Figure 8. The green region is excluded by SN1987A from (35). The blue region is excluded by searches for new spin dependent forces between nuclei. The red line is the projected sensitivity of an NMR style experiment using Xe, the blue line is the sensitivity using ^3He . The dashed lines show the limit from magnetization noise for each sample. The ADMX region shows the part of QCD axion parameter space which has been covered (darker blue) (52) or will be covered in the near future (lighter blue) by ADMX. For full details see (68).

4. Searches for Solar Axions

4.1. Solar Axions

Axions can be produced in the solar interior by the Primakoff conversion of plasma photons into axions in the Coulomb field of charged particles via the generic $a\gamma\gamma$ vertex (88), giving rise to a solar axion flux at the Earth surface (89) of $\Phi_a = g_{10}^2 3.75 \times 10^{11} \text{ cm}^{-2} \text{ s}^{-1}$ (where $g_{10} = g_{a\gamma\gamma}/10^{-10} \text{ GeV}^{-1}$), which corresponds to a fraction of the solar luminosity of $\mathcal{L}_a/\mathcal{L}_\odot = g_{10}^2 1.85 \times 10^{-3}$. These axions have a broad spectral distribution around 1–10 keV, determined by the solar core’s temperature, and usefully parameterized by the following expression (89):

$$\frac{d\Phi_a}{dE} = 6.02 \times 10^{10} \text{ cm}^{-2} \text{ s}^{-1} \text{ keV}^{-1} g_{10}^2 E^{2.481} e^{-E/1.205} \quad (E \text{ in keV}) \quad (22)$$

that is plotted in Fig. 9. This is a robust prediction involving well-known solar physics and

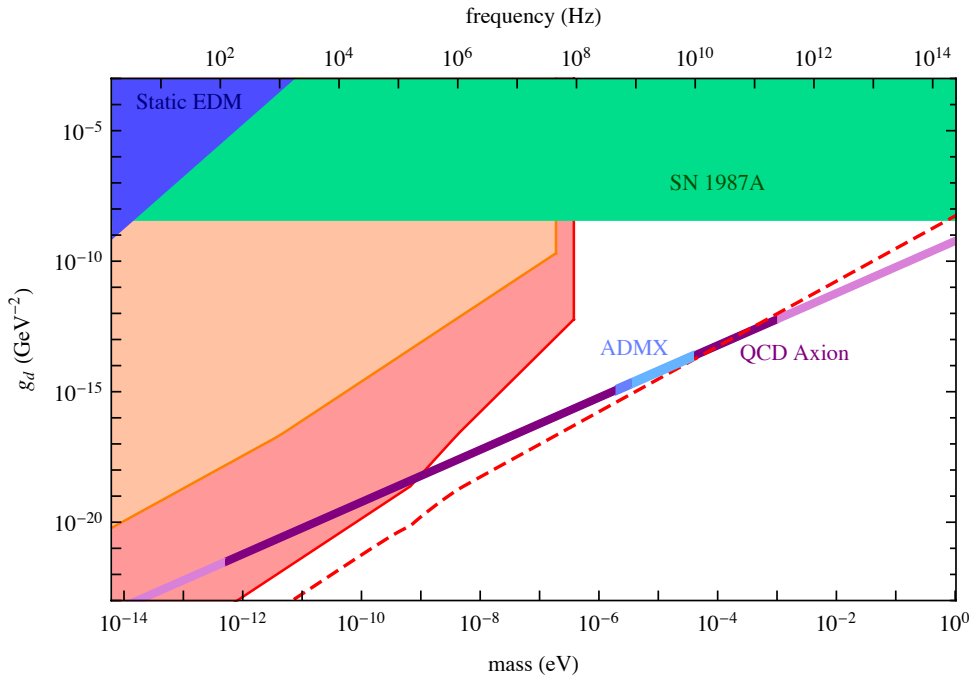


Figure 8

Sensitivity of the CASPER-Electric proposal. Estimated constraints in the ALP parameter space in the EDM coupling g_d (as in Equation 21) vs. the ALP mass. The blue region is excluded by existing, static nuclear EDM searches (68). The solid red and orange regions show projected sensitivity estimates for CASPER-Electric phase 1 and 2 proposals, set by magnetometer noise. The red dashed line shows the limit from magnetization noise of the sample for phase 2. Other regions are as in Figure 7. For full details see (67, 68).

the generic $a\gamma\gamma$ vertex (and thus also valid for more generic ALPs). For particular non-hadronic axion models having a tree-level coupling with electrons g_{aee} , other production channels like axion recombination, bremsstrahlung or Compton (i.e. ABC reactions (90)) should be taken into account. As shown in Fig. 9, if present, this additional solar axion flux could be a factor $\sim 10^2$ larger than the standard Primakoff one, while having lower energies, peaking at ~ 1 keV. However, astrophysical limits on g_{aee} are quite restrictive and largely disfavor the values that could be reached by helioscopes looking at the non-hadronic solar axion flux. In the future IAXO (see Section 4.4) may have sensitivity to ABC solar axions for non-excluded values of g_{aee} . Finally, axion emission in solar nuclear transitions, by virtue of axion-nucleon interactions has also been considered in the literature.

By means of the $a\gamma\gamma$ vertex, solar axions can be efficiently converted back into photons in the presence of an electromagnetic field. In crystalline detectors (91, 92, 93), this effect gives rise to characteristic Bragg patterns that have been searched for as by-products of a number of underground WIMP experiments (94, 95, 96, 97, 98). However, the prospects of this technique have proven limited (99, 100) and do not compete with dedicated helioscope experiments that use a powerful magnet to effect the conversion. Solar axion detection by means of the axioelectric effect in the detector (101, 102, 103, 104, 105) or, for monochro-

matic axions emitted in solar nuclear transitions, the resonant absorption by the same nuclide at the detector (106, 107, 108, 109), have also been considered. While interesting for some specific WISP models, all these techniques remain far from the sensitivity required to probe QCD axion models and/or parameter space not excluded by astrophysics. So far only axion helioscopes have reached relevant QCD axion parameter space.

4.2. Axion helioscopes

The probability that an axion going through the transverse magnetic field B over a length L will convert to a photon is given by (40, 110, 89):

$$P_{a\gamma} = 2.6 \times 10^{-17} \left(\frac{B}{10 \text{ T}} \right)^2 \left(\frac{L}{10 \text{ m}} \right)^2 (g_{a\gamma\gamma} \times 10^{10} \text{ GeV})^2 F$$

where the form factor F accounts for the coherence of the conversion process:

$$F = \frac{2(1 - \cos qL)}{(qL)^2} \quad (23)$$

and q is the momentum transfer. The fact that the axion is not massless implies that the axion and photon states will gradually slip out of phase with distance. The coherence

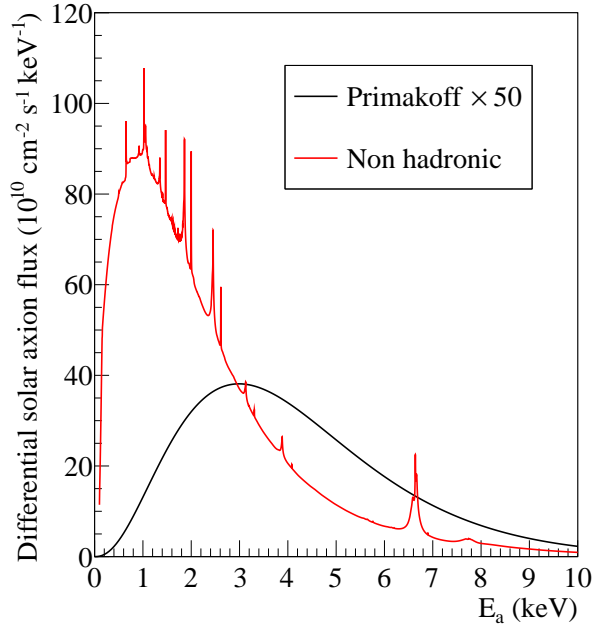


Figure 9

Solar axion flux due to the standard Primakoff conversion (in black) for $g_{a\gamma\gamma} = 10^{-12} \text{ GeV}^{-1}$, as well as from ABC reactions (in red) with $g_{aee} = 10^{-13}$. The Primakoff spectrum has been scaled up by a factor 50 to make both contributions comparable in the plot.

is preserved ($F \simeq 1$) as long as $qL \ll 1$, which for solar axion energies and a magnet length of ~ 10 m happens for axion masses up to $\sim 10^{-2}$ eV, while for higher masses F begins to decrease, and so does the sensitivity of the experiment. To mitigate the loss of coherence, a buffer gas can be introduced into the magnet beam pipes (111, 112) to impart an effective mass to the photons $m_\gamma = \omega_p$ (where ω_p is the plasma frequency of the gas, $\omega_p^2 = 4\pi\alpha n_e/m_e$). For axion masses that match the photon mass, $q = 0$ and full coherence is restored. By changing the pressure of the gas inside the pipe in a controlled manner, the photon mass can be systematically increased and the sensitivity of the experiment can be extended to higher axion masses.

The basic layout of an axion helioscope thus requires a powerful magnet coupled to one or more x-ray detectors. When the magnet is aligned with the Sun, an excess of x-rays at the exit of the magnet is expected, over the background measured at non-alignment periods. This detection concept was first experimentally realized at Brookhaven National Laboratory (BNL) in 1992. A stationary dipole magnet with a field of $B = 2.2$ T and a length of $L = 1.8$ m was oriented towards the setting Sun (113). The experiment derived an upper limit on $g_{a\gamma\gamma}$ (99% CL) $< 3.6 \times 10^{-9}$ GeV $^{-1}$ for $m_a < 0.03$ eV. At the University of Tokyo, a second-generation experiment was built: the SUMICO axion helioscope. Not only did this experiment implement dynamic tracking of the Sun but it also used a more powerful magnet ($B = 4$ T, $L = 2.3$ m) than its BNL predecessor. The bore, located between the two coils of the magnet, was evacuated and higher-performance detectors were installed (114, 115, 116). This new setup resulted in an improved upper limit in the mass range up to 0.03 eV of $g_{a\gamma\gamma}$ (95% CL) $< 6.0 \times 10^{-10}$ GeV $^{-1}$. Later experimental improvements included the additional use of a buffer gas to enhance sensitivity to higher-mass axions.

4.3. CAST

A third-generation experiment, the CERN Axion Solar Telescope (CAST), began data collection in 2003 and is still in operation. The experiment uses a Large Hadron Collider (LHC) dipole prototype magnet with a magnetic field of up to 9 T over a length of 9.3 m (117). CAST is able to follow the Sun for several hours per day using an elevation and azimuth drive. This CERN experiment is the first helioscope to employ x-ray focusing optics for one of its four detector lines (118), as well as low background techniques from detectors in underground laboratories (119, 120, 121). During its observational program from 2003 to 2011, CAST operated first with its magnet bores under vacuum (2003–2004) to probe masses $m_a < 0.02$ eV. No significant signal above background was observed. Thus, an upper limit on the axion-to-photon coupling of $g_{a\gamma\gamma}$ (95% CL) $< 8.8 \times 10^{-11}$ GeV $^{-1}$ was obtained (110, 89). The experiment was then upgraded to be operated with ^4He (2005–2006) and ^3He gas (2008–2011) to obtain continuous, high sensitivity up to an axion mass of $m_a = 1.17$ eV. Data released up to now provide an average limit of $g_{a\gamma\gamma}$ (95% CL) $\lesssim 2.3 \times 10^{-10}$ GeV $^{-1}$, for the higher mass range of 0.02 eV $< m_a < 0.64$ eV (112, 122) and of about $g_{a\gamma\gamma}$ (95% CL) $\lesssim 3.3 \times 10^{-10}$ GeV $^{-1}$ for 0.64 eV $< m_a < 1.17$ eV (123), with the exact value depending on the pressure setting. The envelope of all these limits is shown in Fig. 10. Byproducts of CAST include the search for 14.4 keV solar axions emitted in the M1 transition of ^{57}Fe nuclei (124), the search from MeV axions from ^7Li and $\text{D}(p, \gamma)^3\text{He}$ nuclear transitions (125), the search for solar axions from ABC reactions (126), and the search of more exotic ALP or WISP models, like chameleon particles also potentially emitted in the sun (127, 128). As part of the R&D to assess the technologies for the next

generation axion helioscope IAXO, new lower background Micromegas detectors are actively being developed (120, 121), and a new x-ray telescope coupled with one such detector being built and installed in CAST in 2014. This improved equipment is currently allowing CAST to revisit the ^4He (in 2012) and vacuum (in 2013-15) configurations with an incremental improvement in sensitivity.

So far each subsequent generation of axion helioscopes has resulted in an improvement in sensitivity to the axion-photon coupling constant of about a factor 6 over its predecessors. CAST has been the first axion helioscope to surpass the stringent limits from astrophysics $g_{a\gamma\gamma} \lesssim 10^{-10} \text{ GeV}^{-1}$ over a large mass range and to probe allowed ALP parameter space. As shown in Fig. 10, in the region of higher axion masses ($m_a \gtrsim 0.1 \text{ eV}$), the experiment has entered the band of QCD axion models for the first time and excluded KSVZ axions of specific mass values. CAST is the largest collaboration in axion physics with ~ 70 physicists from about 16 different institutions in Europe and the USA. The scalability of the helioscope technique has been recently proven (129) and a substantial step beyond CAST state-of-the-art is achievable by the proposed International Axion Observatory (IAXO).

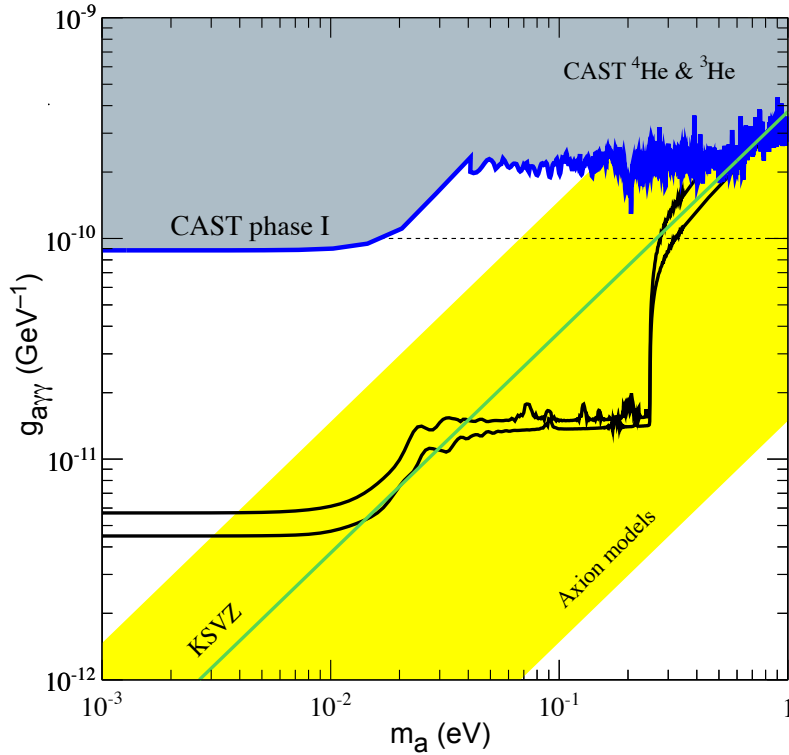


Figure 10

ALP parameter space ($g_{a\gamma\gamma} - m_a$) with the region (yellow band) where QCD axion models lie. Solid areas indicate the regions excluded by current experiments, among them CAST, while the two black lines indicate the expected sensitivity of the future IAXO under two different sets of assumptions.

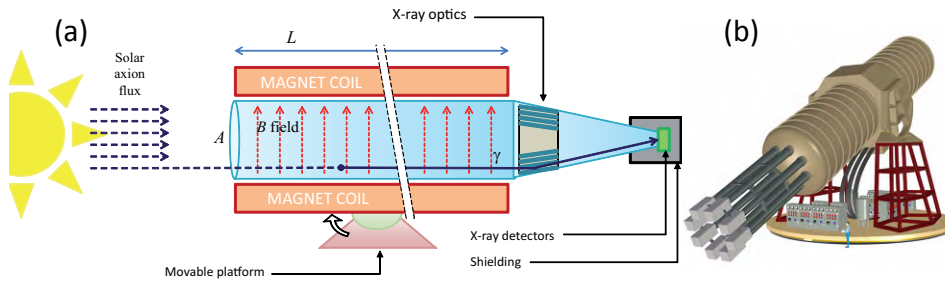


Figure 11

(a) Conceptual arrangement of an enhanced axion helioscope with x-ray focusing. Solar axions are converted into photons by the transverse magnetic field inside the bore of a powerful magnet. The resulting quasi-parallel beam of photons of cross sectional area A is concentrated by appropriate x-ray optics onto a small spot area a in a low background detector. (b) The envisaged design for IAXO includes eight such magnet bores, with their respective optics and detectors.

4.4. IAXO

Going substantially beyond CAST sensitivity is possible only by going to a new magnet, designed and built maximizing the helioscope magnet's figure of merit $f_M = B^2 L^2 A$, proportional to the photon signal from converted axions, where B , L and A are the magnet's field strength, length and cross sectional area, respectively (129). However, for this figure of merit to directly translate into signal-to-noise ratio of the overall experiment for a large aperture magnet, the entire cross sectional area of the magnet must be equipped with x-ray focusing optics. The layout of this *enhanced axion helioscope*, sketched in Figure 11, was proposed (129) as the basis for IAXO. The project is at the point of conceptual design, recently finished (130), and it is now moving into the realization of the technical design report, including some prototyping activities. A recent Letter of Intent (131) to CERN was positively reviewed.

To produce an intense magnetic field over a large volume, and maximize the figure of merit within realistic limits of the different technologies in play, motivates moving to a 25 m long and 5.2 m diameter toroid assembled from 8 coils, producing 2.5 tesla in 8 bores of 600 mm diameter (132). The magnet is supported by a tracking system similar to that of large telescopes. Figure 11 shows the conceptual design of the infrastructure (130). Each of the bores will be equipped with x-ray optics similar to those used on NASA's NuSTAR (133), an x-ray astrophysics satellite with two focusing telescopes that operate in the 3 - 79 keV band, consisting of thousands of thermally-formed glass substrates deposited with multilayer coatings. For IAXO, the multilayer coatings will be designed to match the solar axion spectrum (134). At the focal plane in each of the optics, IAXO will have small gaseous chambers read by pixelated planes of Micromegas, surrounded by active and passive shielding. These detectors are being developed (135, 136, 137, 138) for rare event searches and they show promise to reach background levels below $\sim 10^{-7}$ counts $\text{keV}^{-1} \text{cm}^{-2} \text{s}^{-1}$ in IAXO (120, 121). These levels are achieved by the use of radiopure detector components, shielding, and offline discrimination-algorithms on the 3D event topology in the gas registered by the pixelised readout.

IAXO will have 5 orders of magnitude better signal-to-noise ratio than CAST, which means a sensitivity to $g_{a\gamma\gamma}$ values as low as, or even surpassing, $g_{a\gamma\gamma} \sim 5 \times 10^{-12} \text{GeV}^{-1}$,

for a wide range of axion masses up to about 0.01 eV after ~ 3 years of data taking in vacuum, and around $g_{a\gamma\gamma} \sim 10^{-11} \text{ GeV}^{-1}$ up to about 0.25 eV, after an additional ~ 3 years with the use of a buffer gas in the conversion bores. IAXO will thus deeply enter into unexplored ALP and axion parameter space, as indicated by Fig. 10. At the lowest mass values, IAXO will test ALP models invoked to explain the anomalies in light propagation over astronomical distances. At the high mass part, $m_a > 1 \text{ meV}$, IAXO will explore a broad range of QCD axion models. Its sensitivity would reach axion models with masses down to the few meV range, superseding the SN 1987A energy loss limits on the axion mass and entering parameter space of progressively higher cosmological interest. At the higher part of the range (0.1 - 1 eV) axions are good candidates to the hot DM or additional *dark radiation* that could restore agreement in cosmological parameters. IAXO could also be sensitive to ABC solar axion for non-excluded values of g_{aee} and thus directly test the models invoked to solve the anomalous cooling observed for white dwarfs (139, 140, 38). Additional equipment beyond the baseline configuration (like InGrid detectors, Transition Edge Sensors or low noise CCDs (131)) would extend the detection energy window, and thus explore other less standard physics cases (e.g. the possibility to directly detect the cosmic axion background predicted by some dark radiation models). Finally, the possibility to equip the huge magnetic volume of IAXO with microwave cavities or antennas sensitive to relic axions is being studied, with promising preliminary projections (141) in mass ranges complementary with previous haloscope searches.

5. Purely Laboratory Experiments

Recent years have seen burgeoning interest in experiments searching for axions or other light exotica which do not rely on cosmological or astrophysical sources. This section concerns photon regeneration, colloquially referred to as “Light Shining through Walls” (LSW) by which photons mix with axions (or WISPs more generally), the axions (or WISPs) being regenerated into the photon state on the other side of an optical barrier (Figure 12). For axions, production and regeneration require a transverse magnetic field, but magnets may or may not be required for WISPs in general. We do not attempt to cover the sector of short-range spin dependent forces, which would properly require a review of its own.

The most sensitive LSW experiments today use or plan to use coherent light to provide the photons before the wall. Such light offers the possibility to enhance sensitivities by implementing Fabry-Perots cavities (Figure 12):

- A cavity in front of the wall enables recycling the light shone against the wall and hence to increase the effective light power by a power-built-up factor \mathcal{F}_{PC} .
- A cavity with a power-built-up factor \mathcal{F}_{RC} behind the wall increases the reconversion probability. This technique is called “resonant regeneration”⁴.

The influence of the empty cavity behind the wall is similar to the Purcell effect described first in 1946 (144) (see also (145, 146) for related experiments). The implementation of resonating cavities in LSW experiments has been worked out in more detail in (147, 148, 149). As \mathcal{F} factors of several 10^4 in the optical regime and even several 10^5 for microwaves

⁴The factor \mathcal{F} is in fact the Finesse of the Fabry-Perot resonator. The quality factor, Q of the resonator, which determines the intrinsic line-width, is given by $Q = (l/\lambda)\mathcal{F}$, where l is the length of the cavity, and λ the wavelength.

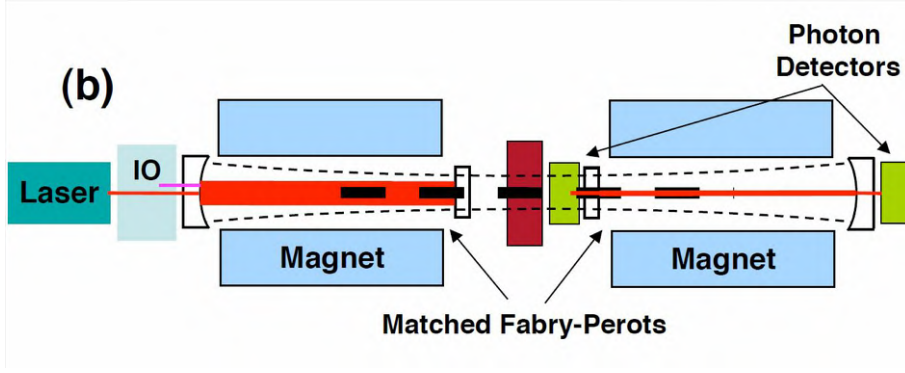


Figure 12

The principle of photon regeneration. Current and future experiments will employ Fabry-Perot cavities both for the production and regeneration regions, and actively locked together, to greatly enhance the experimental sensitivity. The ALPS I experiment has already used such a cavity in the production region (142, 143).

can be reached, resonators allow for significant improvements of experimental sensitivities.

5.1. LSW experiments with microwaves, optical photons and X-rays

Experiments using microwaves usually work in the near-field approximation. One can picture this situation as having a production cavity (PC) emitting a beam of WISPs, where the shape is given by the mode resonating in the cavity. Hence one has to place the detector (regeneration) cavity (RC) somewhere next to the production cavity so that WISPs pass through it. The probability for a photon-WISP-photon oscillation ($\gamma \rightarrow \phi \rightarrow \gamma$) with an effective photon-WISP coupling C_{wisp} in such an installation (150, 151) is given by Eq. 24, where the geometrical form factor G describes the overlap of the modes resonating in the PC and RC. The size of such experiments is essentially given by the microwave wavelength.

$$P_{\gamma \rightarrow \phi \rightarrow \gamma} = |C_{wisp}|^4 \cdot |G|^2 \cdot \mathcal{F}_{PC} \cdot \mathcal{F}_{RC} \quad (24)$$

In a far-field approximation (as realized with optical photons and X-rays) the conversion probability is given by Eq. 25.

$$P_{\gamma \rightarrow \phi \rightarrow \gamma} = \frac{\omega}{\sqrt{\omega^2 - m_\phi^2}} \cdot |C_{wisp}|^4 \cdot \mathcal{F}_{PC} \cdot \mathcal{F}_{RC} \cdot \sin^4 \left(\frac{q \cdot l}{2} \right) \quad (25)$$

Here $q = |n \cdot \omega - \sqrt{\omega^2 - m_\phi^2}|$ with the photon energy ω , the WISP mass m_ϕ and the refractive index n , and l the length of the experiment in front of and behind the wall. For hidden photons and axion-like particles, the couplings are given by Eq. 26:

$$|C_{hp}|^2 = 4\chi^2 \cdot \frac{m_\phi^4}{(m_\phi^2 + 2\omega^2(n-1))^2}; \quad |C_{alp}|^2 = 4 \cdot \frac{(g_{a\gamma\gamma}\omega B)^2}{(m_\phi^2 + 2\omega^2(n-1))^2} \quad (26)$$

with the dimensionless parameter χ and the two-photon coupling strength $g_{a\gamma\gamma}$ with the dimension mass^{-1} . In Eq. 26 it is assumed that the homogeneous magnetic field is oriented

Parameter	Sensitivity	ALPS I	ALPS II	JURA
Effective laser power P_{laser}	$g_{a\gamma\gamma} \propto P_{laser}^{-1/4}$	1 kW	150 kW	1000 kW
\mathcal{F}_{RC}	$g_{a\gamma\gamma} \propto \mathcal{F}_{RC}^{-1/4}$	1	40,000	100,000
Length (B field) l	$g_{a\gamma\gamma} \propto (l)^{-1}$	4.4 m	88 m	286 m
Magnetic field B	$g_{a\gamma\gamma} \propto (B)^{-1}$	5.0 T	5.3 T	13 T

Table 1 Parameters of the ALPS I (142) experiment in comparison to ALPS II (156) and a hypothetical future experiment JURA, just in conceptual phase. The second column shows the dependence of the reachable ALP-photon coupling on the experimental parameters.

perpendicular (parallel) to the E-field of the light wave for interacting with scalar (pseudoscalar) ALPs. The maximal sensitivity is obtained in vacuum with $n = 1$. Following the equations 25 and 26 one arrives at the approximation in equation 27 for $ql \ll 1$ and $n = 1$:

$$P_{\gamma \rightarrow \phi \rightarrow \gamma} = \frac{1}{16} \cdot \mathcal{F}_{PC} \mathcal{F}_{RC} \cdot (g_{a\gamma\gamma} B l)^4 = 6 \cdot 10^{-38} \cdot \mathcal{F}_{PC} \mathcal{F}_{RC} \cdot \left(\frac{g_{a\gamma\gamma}}{10^{-10} GeV^{-1}} \frac{B}{1 T} \frac{l}{10 m} \right)^4 \quad (27)$$

The leading microwave LSW experiment is the CERN Resonant Weakly Interacting sub-eV Particle Search, CROWS (152). It has fully exploited the resonant regeneration technique described above and achieved about the same sensitivity as the optical experiments ALPS I at DESY (142) and OSQAR at CERN (153) which had no cavity behind the wall. ALP-photon couplings around $g_{a\gamma\gamma} = 5 \cdot 10^{-8} GeV^{-1}$ have been probed. While CROWS has searched for ALPs up to its kinematic limit $m_\phi = \omega$, the optical experiments were limited to roughly $m_\phi < 10^{-3} \omega$ due to Eq. 25.

LSW experiments have also been performed with intense X-ray beams available at synchrotron radiation sources (154, 155). Due to the higher photon energy such experiments can probe WISPs up to eV-masses and beyond, but due to the relative low photon number flux and the present impossibility to implement cavities with high power built-ups, X-ray based experiments do not reach the sensitivity of optical or microwave LSW.

5.2. The future of LSW experiments

The most advanced proposal is the ALPS II (156) project being under preparation at DESY (see Figure 13). In Table 1 critical parameters of ALPS I, ALPS II and a future experiment JURA (Joint Undertaking on Research for Axion-like particles) are listed. It is evident that ALPS II has the potential to increase the sensitivity for $g_{a\gamma\gamma}$ by more than three orders of magnitude reaching down to $g_{a\gamma\gamma} = 2 \times 10^{-11} GeV^{-1}$ thus going beyond present-day limits from astrophysics.

To realize an experiment as shown in Figures 12 and 13 both cavities must be mode matched and phase locked. At ALPS II continuous wave infrared light (1064 nm) with a power of up to 35 W is provided by a single-mode single-frequency laser system. Through a curved mirror the laser light is injected into the cavity in front of the wall which is locked via the Pound-Drever-Hall (PDH) sensing scheme (157). This ALPS II cavity is designed for a power build-up $\mathcal{F}_{RC} = 5,000$ providing a circulating power of 150 kW and limiting the power density on the mirrors to 500 kW/cm², about an order of magnitude below their damage thresholds. To allow for locking the cavity behind the wall with the PDH method, a fraction of the 1064 nm light is frequency-doubled to 532 nm in a KTP crystal and fed

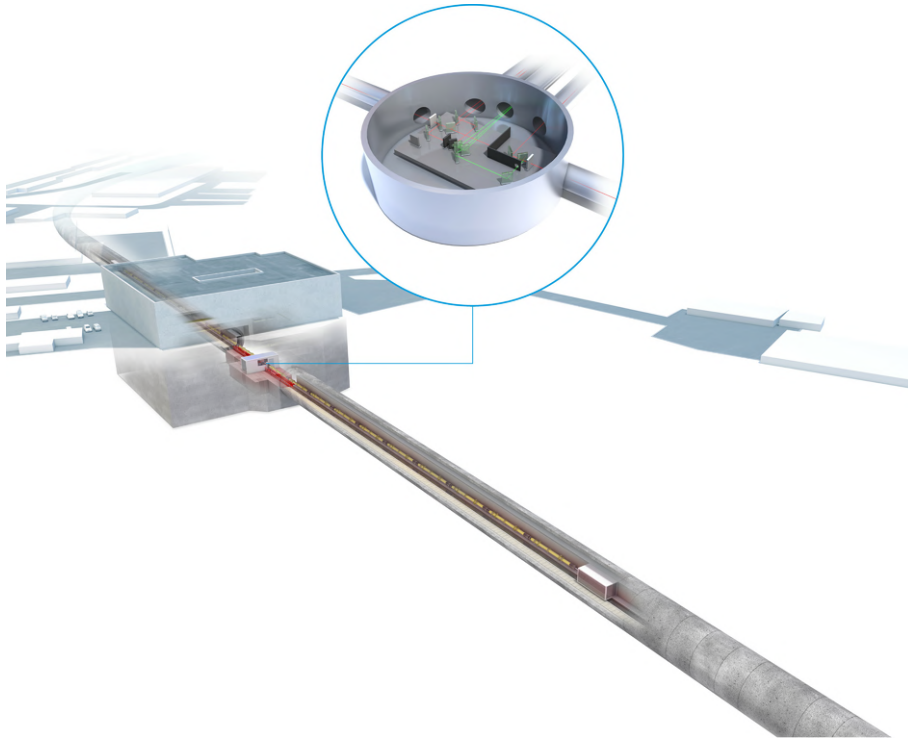


Figure 13

An artist's view of the ALPS II experiment under preparation at DESY: it is planned to install a string of 20 HERA dipole magnets in a straight section of the tunnel of the decommissioned HERA accelerator. The insert sketches parts of the central optics used to align and control the two optical resonators in front of and behind the wall. Copyright 2013, DESY.

into the cavity targeting for a power build-up of $\mathcal{F}_{RC} = 40,000$. For future experiments beyond ALPS II one could think of increasing the circulating light power in front of the wall by another order of magnitude (see also (149)) and to improve on \mathcal{F}_{RC} by advanced seismic isolations of the optical components for example.

ALPS II will use a Transition Edge Sensor (TES) (158, 159) based on a thin superconducting Tungsten film ($25 \mu\text{m} \cdot 25 \mu\text{m} \cdot 20 \text{nm}$) as photon detectors. 1064 nm photons appear as fast pulses with a decay time of about $1.5 \mu\text{s}$. The intrinsic background is below 10^{-4} counts per second, the energy resolution for single infrared photons is better than 10% and the whole system can be operated stably over long time scales (160, 161, 162). Infrared photon detection sensitivity well below mHz rates should be achievable.

An alternative detection scheme is proposed in (149). Here the regeneration cavity is controlled by light which frequency is only shifted by a few free spectral ranges compares to the light in the production cavity (not frequency-doubled as for ALPS II). This approach would allow for a heterodyne detection of the reconverted photons behind the wall by mixing their signal (which would occur at the production cavity's light frequency) with the light controlling the regeneration cavity. In principle any detector background noise can

be rendered negligible in this scheme.

The coupling $g_{a\gamma\gamma}$ that can be reached goes as $(Bl)^{-1}$, but at present LSW experiments have used one or two dipole magnets only. The maximal length of an LSW experiment depends on the aperture of the magnets and the laser beam divergence. This limits the ALPS II setup to a total length of about 200 m for example, which represents 20 HERA dipole magnets⁵. In the far future one could imagine magnet strings based on the dipoles under development at CERN (163, 164) offering a field of about 13 T with an aperture of about 100 mm if the high T_c superconducting inner part is removed (see JURA⁶ in Table 1).

The next generation of laser-based LSW experiments like ALPS II will surpass present day limits on axion-like particles from astrophysics observation, and have the potential to probe a large fraction of the parameter space for axion-like particles as indicated by the cooling of stars or the abnormal high transparency of the universe for TeV photons. However, at present no concept exists on how to access the QCD axion with purely laboratory based experiments. Only once the axion mass is known from dark matter experiments for example, one could think of optimizing the sensitivity of LSW experiments accordingly (165).

6. Summary and Conclusions

Figure 14 schematically represents the current limits on the photon coupling of axions and axion-like particles, and the projected extension of these results with ongoing upgrades within the next five years; companion Figures 7 and 8 summarize the reach of future NMR experiments for lower mass axions through their nucleon coupling. Along with experiments still in the conceptual or prototype phase, these constitute, for the first time, the emergence of a complete strategy to definitively answer the question of the existence of the axion, and its cosmological role, from the neV to meV mass range. It is interesting to note that it has been the mass coverage rate, not the sensitivity of all dark-matter axion searches that has been the limiting factor. If the mass were known virtually any microwave cavity experiment would be able to detect the axion, with sufficient integration time. In fact, if the axion were discovered, it would quickly become a senior undergraduate physics laboratory experiment. The heart of the issue with tuning high-Q experiments is that their exquisite sensitivity accrues as a trade-off for spectral bandwidth, thus necessitating tuning over a decade or more of mass.

The searches for axion-like particles based on axion-photon mixing in the relativistic limit, i.e. helioscope and ‘light shining through walls’ experiments have also achieved an impressive technical sophistication and are now poised for dramatic scale-up from earlier realizations. While their ultimate projections in $g_{a\gamma\gamma}$ might only improve on the best astrophysical limits by an order of magnitude or so, these experiments are extremely important insofar as they have discovery potential for generalized pseudoscalars that may have no origin in Peccei-Quinn symmetry, and for which the microwave cavity experiments, etc. would be irrelevant.

The authors are hopeful, even optimistic the next major review will focus on the properties of the already-discovered axion, and the new field of axion astronomy and cosmology.

⁵The dipole magnets will be straightened to provide a sufficient aperture.

⁶Using 532 nm light instead of 1064 nm would allow a further doubling of the length.

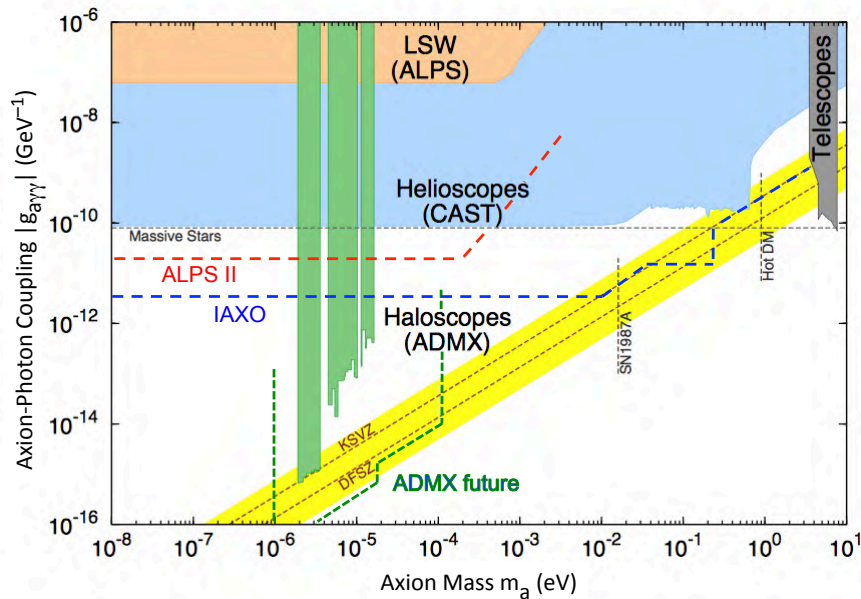


Figure 14

Existing limits on the photon coupling of axions and axion-like particles and the projected coverage of ongoing upgrades for these experiments. Figure adapted from Ref. (39) (the Particle Data Group).

ACKNOWLEDGMENTS

PWG acknowledges the support of NSF grant PHY-1316706, DOE Early Career Award de-sc0012012, the Terman Fellowship, and the Heising-Simons Foundation. I.G.I acknowledges support from the Spanish Ministry of Economy and Competitiveness (MINECO) under contracts FPA2011-24058, FPA2013-41085 and CSD2007-00042 (CPAN project), as well as from the European Research Council under the T-REX Starting Grant ERC-2009-StG-240054 of the IDEAS program of the 7th EU Framework Program. SKL and KvB acknowledge support from the National Science Foundation, under grants PHY-1067242, and PHY-1306729, respectively. We thank J.A. Garcia for the help with figure 9.

LITERATURE CITED

1. Weinberg S. *Phys. Rev. Lett.* 40:223 (1978)
2. Wilczek F. *Phys. Rev. Lett.* 40:279 (1978)
3. Peccei R, Quinn HR. *Phys. Rev. Lett.* 38:1440 (1977)
4. Peccei R, Quinn HR. *Phys. Rev.* D16:1791 (1977)
5. Asztalos SJ, et al. *Ann. Rev. Nucl. Part. Sci.* 56:293 (2006)

6. Rosenberg L, van Bibber K. *Phys. Rept.* 325:1 (2000)
7. Bradley R, et al. *Rev. Mod. Phys.* 75:777 (2003)
8. Kim JE. *Phys. Rept.* 150:1 (1987)
9. Cheng HY. *Phys. Rept.* 158:1 (1988)
10. Turner MS. *Phys. Rept.* 197:67 (1990)
11. Raffelt GG. *Phys. Rept.* 198:1 (1990)
12. Kim JE, Carosi G. *Rev. Mod. Phys.* 82:557 (2010)
13. Khriplovich I, Lamoreaux S. Texts and monographs in physics. Springer-Verlag (1997)
14. Landau L, Lifshitz E. No. Bd. 2 in Course of theoretical physics. Butterworth Heinemann (1975)
15. Baluni V. *Phys. Rev. D* 19:2227 (1979)
16. Crewther R, Vecchia PD, Veneziano G, Witten E. *Phys. Lett. B* 88:123 (1979), erratum: 91, 487(E) (1980)
17. Baker C, et al. *Phys. Rev. Lett.* 97:131801 (2006)
18. Ellis J, Gaillard MK. *Nucl. Phys. B* 150:141 (1979)
19. Khriplovich I, Vainshtein A. *Nucl. Phys. B* 414:27 (1994)
20. Kim JE. *Phys. Rev. Lett.* 43:103 (1979)
21. Shifman MA, Vainshtein A, Zakharov VI. *Nucl. Phys.* B166:493 (1980)
22. Dine M, Fischler W, Srednicki M. *Phys. Lett.* B104:199 (1981)
23. Zhitnitsky A. *Sov. J. Nucl. Phys.* 31:260 (1980)
24. Svrcek P, Witten E. *JHEP* 0606:051 (2006)
25. Jaeckel J, Ringwald A. *Ann. Rev. Nucl. Part. Sci.* 60:405 (2010)
26. Arias P, et al. *JCAP* 1206:013 (2012)
27. Ringwald A. *Phys. Dark Univ.* 1:116 (2012)
28. Meyer M, Horns D, Raue M. *Phys. Rev.* D87:035027 (2013)
29. Rubtsov G, Troitsky S. *JETP Lett.* 100:397 (2014)
30. Ayala A, et al. *Phys. Rev. Lett.* 113:191302 (2014)
31. Miller Bertolami MM, Melendez BE, Althaus LG, Isern J. *JCAP* 1410:069 (2014)
32. Altarelli G. *Nucl. Instrum. Meth.* A742:56 (2014)
33. Feng JL. *Ann. Rev. Nucl. Part. Sci.* 63:351 (2013)
34. Sikivie P. *Lect. Notes Phys.* 741:19 (2008)
35. Raffelt GG. *Lect. Notes Phys.* 741:51 (2008)
36. Isern J, Garcia-Berro E, Torres S, Catalan S. *Astrophys. J.* 682:L109 (2008)
37. Isern J, Garcia-Berro E, Althaus L, Corsico A. *Astron. Astrophys.* 512:A86 (2010)
38. Corsico A, et al. *JCAP* 1212:010 (2012)
39. Olive K, et al. *Chin. Phys.* C38:090001 (2014)
40. Sikivie P. *Phys. Rev. Lett.* 51:1415 (1983)
41. Sikivie P. *Phys. Rev.* D32:2988 (1985)
42. Dicke R. *Rev. Sci. Instr.* 17:268 (1946)
43. Sikivie P. *Phys. Lett.* B695:22 (2011)
44. van Bibber K, Kinion S. *Phil. Trans. Roy. Soc. Lond.* A361:2553 (2003)
45. De Panfilis S, et al. *Phys. Rev. Lett.* 59:839 (1987)
46. Wuensch W, et al. *Phys. Rev.* D40:3153 (1989)
47. Hagemann C, Sikivie P, Sullivan N, Tanner D. *Phys. Rev.* D42:1297 (1990)
48. Tada M, et al. *Phys. Lett. A* 349:488 (2006)
49. Muck M, et al. *Applied Physics Letters* 72 (1998)
50. Muck M, et al. *Appl. Phys. Lett.* 75:3545 (1999)
51. Muck M, Clarke J. *Journal of Applied Physics* 88 (2000)
52. Asztalos S, et al. *Phys. Rev. Lett.* 104:041301 (2010)
53. Hoskins J, et al. *Phys. Rev.* D84:121302 (2011)
54. Shokair T, et al. *Int. J. Mod. Phys.* A29:1443004 (2014)

55. Castellanos-Beltran MA, Lehnert KW. *Applied Physics Letters* 91: (2007)
56. Castellanos-Beltran MA, et al. *Nat Phys* 4:929 (2008)
57. Xi X, et al. *Phys. Rev. Lett.* 105:257006 (2010)
58. Mallet F, et al. *Phys. Rev. Lett.* 106:220502 (2011)
59. Lamoreaux S, van Bibber K, Lehnert K, Carosi G. *Phys. Rev.* D88:035020 (2013)
60. Schuster DI, et al. *Nature* 445:515 (2007)
61. Wallraff A, et al. *Nature* 431:162 (2004)
62. Chen YF, et al. *Phys. Rev. Lett.* 107:217401 (2011)
63. Rybka G, Wagner A arXiv:1403.3121 [physics.ins-det] (2014)
64. Sikivie P, Sullivan N, Tanner D. *Phys. Rev. Lett.* 112:131301 (2014)
65. Baker OK, et al. *Phys. Rev.* D85:035018 (2012)
66. Horns D, et al. *JCAP* 1304:016 (2013)
67. Budker D, et al. *Phys. Rev.* X4:021030 (2014)
68. Graham PW, Rajendran S. *Phys. Rev.* D88:035023 (2013)
69. Linde AD. *Phys. Lett.* B201:437 (1988)
70. Wilczek F arXiv:1204.4683 [hep-th] (2012)
71. Arvanitaki A, Baryakhtar M, Huang X arXiv:1411.2263 [hep-ph] (2014)
72. Arvanitaki A, Dubovsky S. *Phys. Rev.* D83:044026 (2011)
73. Arvanitaki A, et al. *Phys. Rev.* D81:123530 (2010)
74. Graham PW, Rajendran S. *Phys. Rev.* D84:055013 (2011)
75. Stadnik Y, Flambaum V. *Phys. Rev.* D89:043522 (2014)
76. Stadnik YV, Flambaum VV arXiv:1409.2986 [hep-ph] (2014)
77. Hong J, Kim JE. *Phys. Lett.* B265:197 (1991)
78. Roberts B, et al. *Phys. Rev.* D90:096005 (2014)
79. Roberts B, et al. *Phys. Rev. Lett.* 113:081601 (2014)
80. Moody J, Wilczek F. *Phys. Rev.* D30:130 (1984)
81. Vasilakis G, Brown J, Kornack T, Romalis M. *Phys. Rev. Lett.* 103:261801 (2009)
82. Burghoff M, et al. *J. Phys. Conf. Ser.* 295:012017 (2011)
83. Ledbetter M, Romalis M, Jackson-Kimball D. *Phys. Rev. Lett.* 110:040402 (2013)
84. Heil W, et al. *Annalen Phys.* 525:539 (2013)
85. Tullney K, et al. *Phys. Rev. Lett.* 111:100801 (2013)
86. Arvanitaki A, Geraci AA. *Phys. Rev. Lett.* 113:161801 (2014)
87. Nelson AE, Scholtz J. *Phys. Rev.* D84:103501 (2011)
88. Raffelt GG. *Ann. Rev. Nucl. Part. Sci.* 49:163 (1999)
89. Andriamonje S, et al. *JCAP* 0704:010 (2007)
90. Redondo J. *JCAP* 1312:008 (2013)
91. Buchmüller W, Hoogeveen F. *Phys. Lett.* B237:278 (1990)
92. Paschos EA, Zioutas K. *Phys. Lett.* B323:367 (1994)
93. Creswick RJ, et al. *Phys. Lett.* B427:235 (1998)
94. Avignone F. T. I, et al. *Phys. Rev. Lett.* 81:5068 (1998)
95. Morales A, et al. *Astropart. Phys.* 16:325 (2002)
96. Bernabei R, et al. *Phys. Lett.* B515:6 (2001)
97. Ahmed Z, et al. *Phys. Rev. Lett.* 103:141802 (2009)
98. Armengaud E, et al. arXiv:1307.1488 [astro-ph.CO] (2013)
99. Cebrián S, et al. *Astropart. Phys.* 10:397 (1999)
100. Avignone III FT, Creswick RJ, Nussinov S arXiv:1002.2718 [astro-ph.CO] (2010)
101. Ljubicic A, Kekez D, Krecak Z, Ljubicic T. *Phys. Lett.* B599:143 (2004)
102. Derbin A, et al. *Phys. Rev.* D83:023505 (2011)
103. Derbin A, Muratova V, Semenov D, Unzhakov E. *Phys. Atom. Nucl.* 74:596 (2011)
104. Derbin A, Drachnev I, Kayunov A, Muratova V. *JETP Lett.* 95:379 (2012)
105. Bellini G, et al. *Phys. Rev.* D85:092003 (2012)

106. Moriyama S. *Phys. Rev. Lett.* 75:3222 (1995)
107. Krcmar M, et al. *Phys. Lett.* B442:38 (1998)
108. Krcmar M, et al. *Phys. Rev.* D64:115016 (2001)
109. Derbin A, et al. *Phys. Lett.* B678:181 (2009)
110. Zioutas K, et al. *Phys. Rev. Lett.* 94:121301 (2005)
111. van Bibber K, McIntyre PM, Morris DE, Raffelt GG. *Phys. Rev.* D39:2089 (1989)
112. Arik E, et al. *JCAP* 0902:008 (2009)
113. Lazarus DM, et al. *Phys. Rev. Lett.* 69:2333 (1992)
114. Inoue Y, et al. *Phys. Lett.* B536:18 (2002)
115. Moriyama S, et al. *Phys. Lett.* B434:147 (1998)
116. Inoue Y, et al. *Phys. Lett.* B668:93 (2008)
117. Zioutas K, et al. *Nucl. Instrum. Meth.* A425:480 (1999)
118. Kuster M, et al. *New J. Phys.* 9:169 (2007)
119. Abbon P, et al. *New J. Phys.* 9:170 (2007)
120. Aune S, et al. *JINST* 9:P01001 (2014)
121. Aune S, et al. *JINST* 8:C12042 (2013)
122. Arik E, et al. *Phys. Rev. Lett.* 107:261302 (2011)
123. Arik M, et al. *Phys. Rev. Lett.* 112:091302 (2014)
124. Andriamonje S, et al. *JCAP* 0912:002 (2009)
125. Andriamonje S, et al. arXiv:0904.2103 [hep-ex] (2009)
126. Barth K, et al. *JCAP* 1305:010 (2013)
127. Brax P, Lindner A, Zioutas K. *Phys. Rev.* D85:043014 (2012)
128. Baum S, et al. arXiv:1409.3852 [astro-ph.IM] (2014)
129. Irastorza IG, et al. *JCAP* 1106:013 (2011)
130. Armengaud E, et al. *JINST* 9:T05002 (2014)
131. Irastorza IG. The International Axion Observatory IAXO. Letter of Intent to the CERN SPS committee. Tech. Rep. CERN-SPSC-2013-022. SPSC-I-242, CERN, Geneva (2013)
132. Shilon I, Dudarev A, Silva H, Kate H. *IEEE Trans. Appl. Supercond.* 23 (2012)
133. Harrison FA, et al. *Astrophysical Journal* 770:103 (2013)
134. Jakobsen AC, Pivovarov MJ, Christensen FE. *Proc. SPIE* 8861:886113 (2013), proc. SPIE 8861, Optics for EUV, X-Ray, and Gamma-Ray Astronomy VI, 886113 (2013)
135. Irastorza I, et al. *EAS Publications Series* 53:147 (2012)
136. Dafni T, et al. *J. Phys. Conf. Ser.* 375:022003 (2012)
137. Dafni T, et al. *J. Phys. Conf. Ser.* 347:012030 (2012)
138. T-REX project web page: <http://gifna.unizar.es/trex/>
139. Isern J, Catalan S, Garcia-Berro E, Torres S. *J.Phys.Conf.Ser.* 172:012005 (2009)
140. Corsico AH, et al. arXiv:1205.6180 [astro-ph.SR] (2012)
141. J. Redondo, talk at Patras Workshop on Axions, WIMPs and WISPs, CERN, June 2014. <http://axion-wimp2014.desy.de/>
142. Ehret K, et al. *Phys. Lett.* B689:149 (2010)
143. Ehret K, et al. *Nucl. Instrum. Meth.* A612:83 (2009)
144. Purcell E. *Phys. Rev.* 69:681 (1946)
145. Haroche S, Kleppner D. *Phys. Today* 42:24 (1989)
146. Haroche S. *Phys. World* 4N3:33 (1991)
147. Hoogeveen F, Ziegenhagen T. *Nucl. Phys.* B358:3 (1991)
148. Fukuda Y, Kohmoto T, Nakajima Si, Kunitomo M. *Prog. Cryst. Growth Charact.Mater.* 33:363 (1996)
149. Mueller G, Sikivie P, Tanner DB, van Bibber K. *Phys. Rev.* D80:072004 (2009)
150. Jaeckel J, Ringwald A. *Phys. Lett.* B659:509 (2008)
151. Caspers F, Jaeckel J, Ringwald A. *JINST* 4:P11013 (2009)
152. Betz M, et al. *Phys. Rev.* D88:075014 (2013)

153. Ballou R, et al. arXiv:1410.2566 [hep-ex] (2014)
154. Battesti R, et al. *Phys. Rev. Lett.* 105:250405 (2010)
155. Inada T, et al. *Phys. Lett.* B722:301 (2013)
156. Bähre R, et al. arXiv:1302.5647 [physics.ins-det] (2013)
157. Black E. *Am. J. of Phys.* 69:79 (2001)
158. Lita A.E. ea. *Proc. SPIE (Advanced Photon Counting Techniques IV)* 76810D (2010)
159. Miller A.J. ea. *Optics Express Vol. 19* 10:9102 (2011)
160. Dreyling-Eschweiler J DESY-THESIS:2014-016 (2014)
161. Dreyling-Eschweiler J arXiv:1409.6992 [physics.ins-det] (2014)
162. Dreyling-Eschweiler J. ea. *submitted to Journal of Modern Optics* (2014)
163. Bottura L, de Rijk G, Rossi L, Todesco E. *IEEE Trans. Appl. Supercond.* 22:4002008 (2012)
164. Todesco E, Bottura L, de Rijk G, Rossi L. *IEEE Trans. Appl. Supercond.* 24:4004306 (2014)
165. Arias P, Jaeckel J, Redondo J, Ringwald A. *Phys. Rev. D* 82:115018 (2010)